Microfluidic Chip to Produce Temperature Jumps for Electrophysiology

ARTICLE *in* ANALYTICAL CHEMISTRY · MAY 2008

Impact Factor: 5.64 · DOI: 10.1021/ac702169t · Source: PubMed

Anal. Chem. **2008,** *80,* 2447−2451

Microfluidic Chip to Produce Temperature Jumps for Electrophysiology

Thomas Pennell,† Thomas Suchyna,‡ Jianbin Wang,† Jinseok Heo,† James D. Felske,† Frederick Sachs,‡ and Susan Z. Hua*,†,‡

Department of Mechanical and Aerospace Engineering, State University of New York—Buffalo, Buffalo, New York 14260, and Department of Physiology and Biophysics, State University of New York—Buffalo, Buffalo, New York 14214

We developed a microfluidic chip that provides rapid temperature changes and accurate temperature control of the perfusing solution to facilitate patch-clamp studies. The device consists of a fluid channel connected to an accessible reservoir for cell culture and patch-clamp measurements. A thin-film platinum heater was placed in the flow channel to generate rapid temperature change, and the temperature was monitored using a thin-film resistor. We constructed the thermal chip using SU-8 on a glass wafer to minimize the heat loss. The chip is capable of increasing the solution temperature from bath temperature (20 °C) to 80 °C at an optimum heating rate of 0.5 °C/ms. To demonstrate the ability of the thermal chip, we have conducted on-chip patch-clamp recordings of temperature-sensitive ion channels (TRPV1) transfected HEK293 cells. The heat-stimulated currents were observed using whole-cell and cell-attached patch configurations. The results demonstrated that the chip can provide rapid temperature jumps at the resolution of single-ion channels.

Temperature has strong effects on cell function and cellular processes. In addition to the general thermal effects on ion channel kinetics, the discovery of heat-gated ion channels in neurons[1] has focused interest on thermosensing pathways.[2,3] Neurons detect and react to heat via thermal-sensitive ion channels. The quantitative investigation of channel activity requires controlled thermal stimuli.[4,5] Commercially available instruments do not provide sufficient speed to resolve the kinetic response to steps in temperature. Most existing heater devices, such as the ITO (indium tin oxide)-coated glass heater or focused laser apparatus can provide fast rise time of the temperature; however, the fall time is limited by thermal diffusion due to the size of the source, so only small volumes can cool fast. A dual-channel flow can produce faster temperature change; however, this requires moving parts and the actual temperature at the cell is not under tight control.[8] Here we present a microfluidic thermal chip that enables rapid temperature change with accurate temperature control.

Microfluidic devices offer the advantage of precise thermal input and, because of their small volume, rapid temperature changes. The resistive heater responds rapidly,[6,7] requires simple fabrication, and offers minimum interference with picoamp−nanoamp patch-clamp electrical signals. Several microheater devices have been built on silicon chips using MEMS (microelectromechanical systems) technology for various microfluidic applications.[9] Since the thermal conductivity of silicon is relatively large and results in high substrate heat losses, significant effort has been focused on isolating the heating element from the substrate. Typically, a thin silicon nitride membrane with an air gap has been used to isolate the heater from the silicon substrate. With the use of this approach, a fluidic chamber with an integrated platinum heater has been demonstrated for precise temperature control with low power consumption.[7] Rapid temperature cycling has also been achieved by controlling the heat flow via various thermal designs of the heating chamber.[10−13] On the other hand, the high thermal conductivity of silicon has been utilized by constructing arrays of micromachined silicon posts which enabled efficient heat dissipation into a fluidic channel through the microfinned surfaces of the channel.[14] Although the performance of silicon-based heaters has been demonstrated, their complicated fabrication process has limited their applications. Recently, glass substrate has been used to construct polymerase chain reaction (PCR) reactors showing faster thermal cycling.[15,16]

* Corresponding author. Phone: 716-645-2593 ext. 2358. Fax: 716-645-3875. E-mail: zhua@eng.buffalo.edu.

† Department of Mechanical and Aerospace Engineering.

‡ Department of Physiology and Biophysics.

(1) Cesare, P.; McNaughton, P. *Proc. Natl. Acad. Sci. U.S.A.* **1996**, *93*, 15435−15439.
(2) Green, B. G. *J. Neurobiol.* **2004**, *61*, 13−29.
(3) Tominaga, M.; Caterina, M. J. *J. Neurobiol.* **2004**, *61*, 3−12.
(4) Dittert, I.; Benedikt, J.; Vyklicky, L.; Zimmermann, K.; Reeh, P. W.; Vlachova, V. *J. Neurosci. Methods* **2006**, *151*, 178−185.
(5) Reid, G.; Amuzescu, B.; Zech, E.; Flonta, M. L. *J. Neurosci. Methods* **2001**, *111*, 1−8.
(6) Rebrov, E. V.; Duinkerke, S. A.; de Croon, M. H. J. M.; Schouten, J. C. *Chem. Eng. J.* **2003**, *4139*, 1−16.
(7) Lao, A. I. K.; Lee, T. M. H.; Hsing, I.; Ip, N. Y. *Sens. Actuators, A* **2000**, *84*, 11−17.
(8) Sachs, F. *Biophys. J.* **1999**, *77*, 682−690.
(9) Woodley, A. T.; Hadley, D.; Landre, P.; deMello, A. J.; Mathies, R. A.; Northrup, M. A. *Anal. Chem.* **1996**, *68*, 4081−4086.
(10) Daniel, J. H.; Iqbal, S.; Millington, R. B.; Moore, D. F.; Lowe, C. R.; Leslie, D. L.; Lee, M. A.; Pearce, M. J. *Sens. Actuators, A* **1998**, *71*, 81−88.
(11) Poser, S.; Schulz, T.; Dillner, U.; Baier, V.; Kohler, J. M.; Schimkat, D.; Mayer, G.; Seibert, A. *Sens. Actuators, A* **1997**, *62*, 672−675.
(12) Losey, M. W.; Jackman, R. J.; Firebaugh, S. L.; Schmidt, M. A.; Jensen, K. F. *J. Microelectromech. Syst.* **2002**, *11*, 709−717.
(13) Lee, M.; Wong, M.; Zohar, Y. *J. Microelectromech. Syst.* **2003**, *12*, 138−146.
(14) Tian, W. C.; Pang, S. W. *J. Vac. Sci. Technol., B* **2002**, *20*, 1008−1012.
(15) Lagally, E. T.; Emrich, C. A.; Mathies, R. A. *Lab Chip* **2001**, *1*, 102−107.
(16) El-Ali, J.; Perch-Nielsen, I. R.; Poulsen, C. R.; Bang, D. D.; Telleman, P.; Wolff, A. *Sens. Actuators, A* **2004**, *110*, 3−10.

10.1021/ac702169t CCC: $40.75
Published on Web 02/27/2008

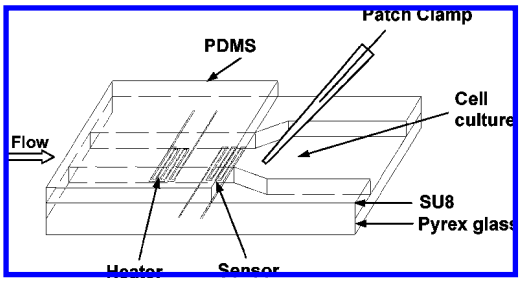

Figure 1. Schematic drawing of the thermal chip.

In this study, we have constructed a microfluidic thermal chip using SU-8 polymer on a glass substrate. The low thermal conductivity of both glass and SU-8 minimize the substrate heat losses, thereby enabling large, rapid, temperature changes. The temperature was monitored using a thin-film resistive sensor at the outlet of the flow channel. We tested the thermal chip performance by recording patch-clamp current from the temperature-sensitive ion channels, TRPV1,[17] transfected HEK293 cells. The thermal chip is very simple to fabricate, capable of heating solution rapidly with minimal power, and is cost-effective. With the use of this simple technique, various on-chip thermal devices can be developed for controlling chemical reactions and temperature-dependent biomedical assays.

EXPERIMENTAL SECTION

Design Principles. The thermal chip consists of a fluid channel connected to a reservoir accessible for making patch-clamp measurements on individual cells. Figure 1 is a schematic of the thermal chip. A thin-film platinum heater and a thin-film platinum resistive sensor were placed strategically along the fluid channel. The heat generated from the heater is carried downstream to the testing region by the passing flow, and the temperature change at the cell location is monitored using the resistive sensor.

The following requirements influenced the design of the heater with respect to its speed of response and its thermal efficiency. (1) Maximize the fraction of heat dissipated by the heater which goes into the fluid by minimizing substrate heat losses. For this purpose we used Pyrex glass as the substrate and a photosensitive polymer (SU-8) to construct the fluid channel. Both glass and SU-8 have relatively low thermal conductivities, 1.1 and 0.2 W/m·K, respectively. In addition, these materials require only very simple fabrication processes in comparison with standard bulk machining. (2) Minimize the diffusion length from the heater to the body of the fluid. A 1:10 ratio of height to width of the fluid channel was chosen in order to minimize the diffusion length. (3) Reduce the length of the heating zone along the flow direction. The heater width was confined to 100 μm in order to obtain an optimum rise time of the fluid temperature. (4) Minimize the heat loss through lead wires. To achieve this, a "zigzag" heater wire design was used in which the resistance in the heating region is 10 times higher than the total resistance from the lead wire on the top of the chip.

Microfabrication. A scanning electron microscopy (SEM) micrograph of the prototype thermal chip is shown in Figure 2A.

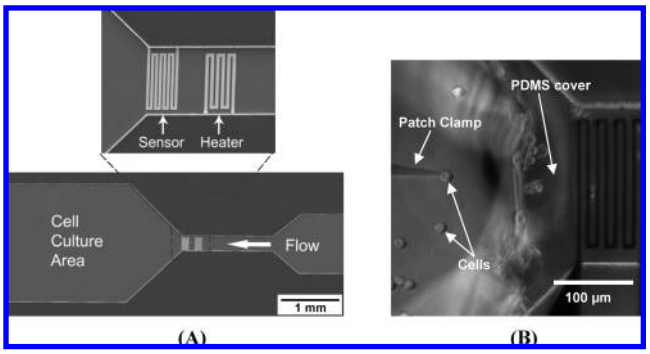

Figure 2. (A) SEM micrograph of the microfluidic thermal chip. The enlarged image shows the configuration of the thin-film platinum heater and sensor along the fluid channel. (B) Optical micrograph of a patched cell on chip. The image was taken prior to patch-clamp recording.

The enlarged image shows its heating and sensing regions. The microfluidic channel is 250 μm wide and 25 μm deep with an inlet port at one end and is connected to an open reaction reservoir. A platinum heater and a thin-film resistive sensor (located 100 μm downstream from the heater) were placed along the channel. With the use of the lift-off technique, a 7.5 nm thick tantalum seed layer followed by a 200 nm thick thin-film platinum electrodes were deposited on the glass wafer by e-beam deposition. The line width of the heater and sensor electrodes were 12 and 10 μm, which produced a room-temperature resistance of ~100 Ω for the heater and ~150 Ω for the sensor, respectively. In order to reduce the amount of interference between the heater and the patch-clamp amplifier, a 1 μm oxide layer was deposited on the entire wafer using the low-pressure chemical vapor deposition (LPCVD) method. This step was followed by a photolithography process to pattern small windows on the electrodes close to the end; the oxide layer in the windows was removed using buffered oxide etch (BHF) in order to make electrical contact. The fluidic channel was constructed using SU-8 photoresist following the standard protocol. A programmed temperature ramp-up hard-baking process was applied after lithography; this process also helped to heal the microcracks in the SU-8 structure. Precured poly(dimethylsiloxane) (PDMS) films were used to seal the fluidic channel. Silicone tubing with 0.79 mm i.d. was embedded into the PDMS at the desired position during the curing process; it was then cut open to form inlet and outlet ports. Prior to experiments, the PDMS films were placed on the surface of the SU-8 channel with the open holes aligned to the inlet port of the channel.

Experimental Setup. Various flow rates through the fluidic channel were achieved by varying the hydraulic pressure at the inlet. A syringe connected to the inlet was raised to various heights, and the flow rate was calibrated by injecting a small bubble and measuring its movement. A function generator was connected to the heater with the voltage pulse ranging from 0.8 to 6 V. The temperature was monitored by the thin-film resistive sensor through use of a phase-locked amplifier with a voltage 0.06 Vpp at 400 Hz.

Cell Culture. HEK293 cells were grown in Dulbecco's modified Eagle's medium (DMEM) containing fetal bovine serum and penicillin−streptomycin for 2−3 days in a 50 mL cell culture flask. When the cells were ~50% confluent in the flask, they were

(17) Okumura, R.; Shima, K.; Muramatsu, T.; Nakagawa, K.; Shimono, M.; Suzuki, T.; Magloire, H.; Shibukawa, Y. *Arch. Histol. Cytol.* **2005**, *68*, 251−257.

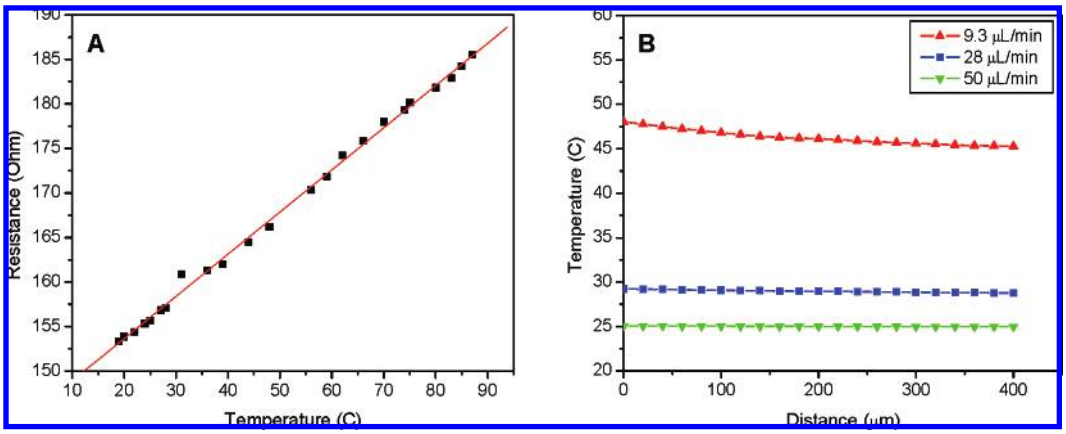

Figure 3. (A) Calibration of the correlation between resistance and temperature of the thin-film thermal sensor. (B) CFD simulation of fluid temperature drop from the sensor position to 400 μm into the cell culture reservoir along the centerline.

cotransfected with 1.3 μg of GFP and 2.8 μg of TRPV-1 plasmid DNAs by using transfection reagent (FuGene 6, Roche Applied Science, IN) according to the manufacturer's protocol. The wild-type HEK cells were also cultured without a transfection procedure for the control experiment. The cells were kept in the incubator for another 24 h. They were then transferred to the reaction reservoir on the microfluidic chip. We filled the reservoir as well as the perfusion fluidic channel and the tubing with DMEM media. The chip was stored in the incubator for 30−90 min so that the cells could attach to the bottom surface of the reservoir. During the patch-clamp experiments, we compared TRPV-1 expressing HEK293 cells with wild-type judged by the fluorescence of GFP.

Patch Clamp. Whole-cell currents were measured by forming a seal on HEK cells with a patch electrode. The patch of membrane separating the inside of the cell from the inside of the patch electrode was then broken by applying suction via the pipet and a large sinusoidal current. This causes the patch membrane to break while maintaining the electrical seal with the glass allowing electrical access to the inside of the cell and control of the voltage across the cell membrane. An Axopatch 200B (Axon Instruments, CA) was used for patch clamping, and experimental protocols and data acquisition were controlled by Axon Instruments pClamp9 software via a Digidata 1322A acquisition system. Currents were sampled at 10 kHz and low-pass-filtered at 2 kHz through the 4-pole Bessel filter on the Axopatch 200B. All potentials are defined as membrane potentials with respect to the extracellular surface. Electrodes were pulled on a HEKA PIP 5 pipet puller (Digitimer, Hertfordshire, U.K.), painted with Sylgard 184 (Dow Corning Corp., Midland, MI) and fire-polished. Electrodes were filled with KCl saline (140 mM KCl, 5 mM EGTA, 2 mM $MgSO_4$, 10 mM HEPES, pH 7.3) and had resistances ranging from 4 to 8 MΩ. Bath saline consisted of 140 mM NaCl, 5 mM KCl, 2 mM $CaCl_2$, 0.5 mM $MgCl_2$, 6 mM glucose, and 10 mM HEPES, pH 7.3. Figure 2B shows an optical micrograph of a patched cell on chip prior to the measurement. Since the cells were loosely attached on the bottom of the reservoir after 30−90 min of incubation, the patched cell can be moved close to the channel outlet for testing.

RESULTS AND DISCUSSION

Thermal Sensor Calibration. The thermal sensor was calibrated by submersing the chip in a bath of deionized water on a hot plate. The temperature was changed and stabilized at the desired values, and the sensor resistance was measured and compared with the readings from a thermometer. A calibration curve is shown in Figure 3A. A linear relationship between thin-film resistance and temperature was obtained. The temperature coefficient of resistance was calculated as 0.3% ($°C^{-1}$). This result is lower than the coefficient for bulk platinum but is consistent with that of other thin-film-based Pt resistors.[18] At least five chips were characterized from each wafer for a total six wafers. The variations in resistance values are within 5% for the chips from the same wafer and less than 10% from wafer to wafer.

The extent of the temperature variation between the thermal sensor and the cell sample was estimated using fluid dynamics software (Coventor). A numerical model was developed having the same dimensions and the same material properties as the actual chip. A heater power of 113 mW and various flow rates of 9.3, 28, and 50 μL/min were selected in the simulation to match actual experimental conditions; since the diffusion equation is linear in temperature, the results can be readily extended to other heater powers. Figure 3B shows the drop in temperature predicted along the axis of symmetry of the outflow stream from the sensor position (the origin in Figure 3B) to 400 μm downstream. The maximum temperature drop was 2.7 °C for the lowest flow rate at a distance 400 μm downstream of the outlet. For the flow rates used in the patch-clamp experiment (~11 μL/min), we predicted a temperature drop of less than 2 °C.

The local time and space gradient in temperature is also expected as in any small volume system. This needs to be evaluated on each preparation since the effect will depend on the sensitivity of the system under study. For lower sensitivity, the steady-state temperature response can be achieved by perfusion with a flow path that is large compared to the cell. If the sensitivity is high, a small preparation, for example, an excised patch containing the channel or other molecules of interest, is preferred in order to reduce the spatial gradient across the sample. Correcting for this can be done precisely in the case of ion channels by precalibrating the unitary channel conductance versus temperature.[19] In the case of multiple channels patches, this can be done by using voltage pulses to estimate the instantaneous

(18) Eriksson, P.; Andersson, J. Y.; Stemme, G. *J. Microelectromech. Syst.* **1997**, *6*, 55−61.

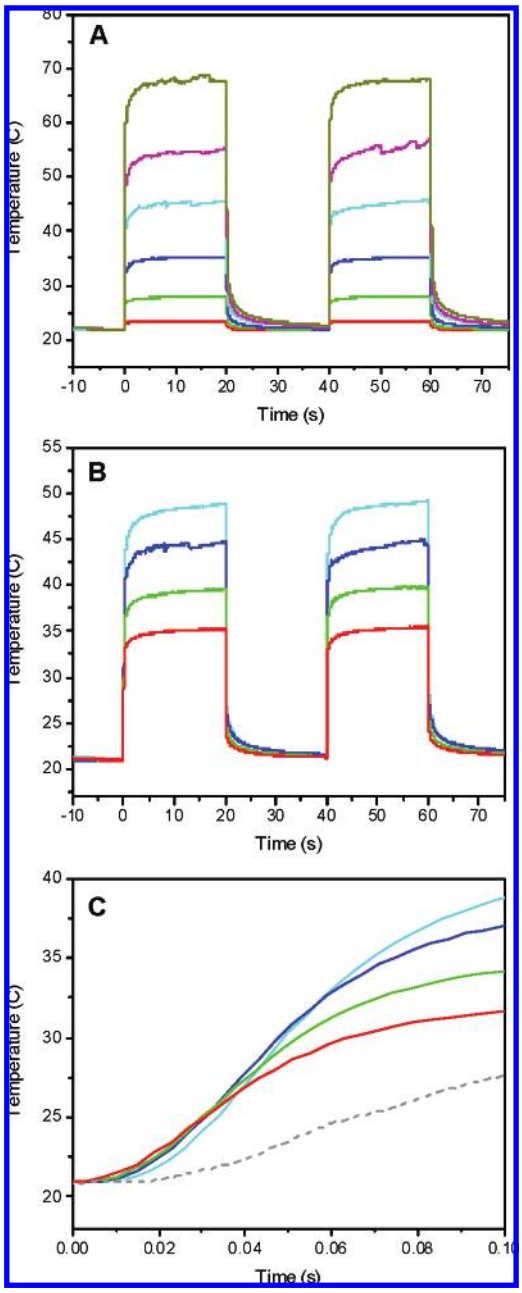

Figure 4. (A) Measured fluid temperature at the outlet of the channel in response to various heater powers. A series of heater powers of 7.2 (red), 28.4 (green), 64 (blue), 112 (cyan), 176 (magenta), and 256 mW (dark yellow) were applied. The flow rate in the fluidic channel was fixed at 16.2 μL/min. (B) Measured temperature change at the outlet of the channel for various flow rates, 12.3 (cyan), 16.2 (blue), 21.9 (green), and 33.9 μL/min (red). A voltage pulse of 3.2 V, 20 s wide, was applied to the heater to generate power of 113 mW. (C) Zoomed view of temperature changes at the beginning of the applied heater power pulse.

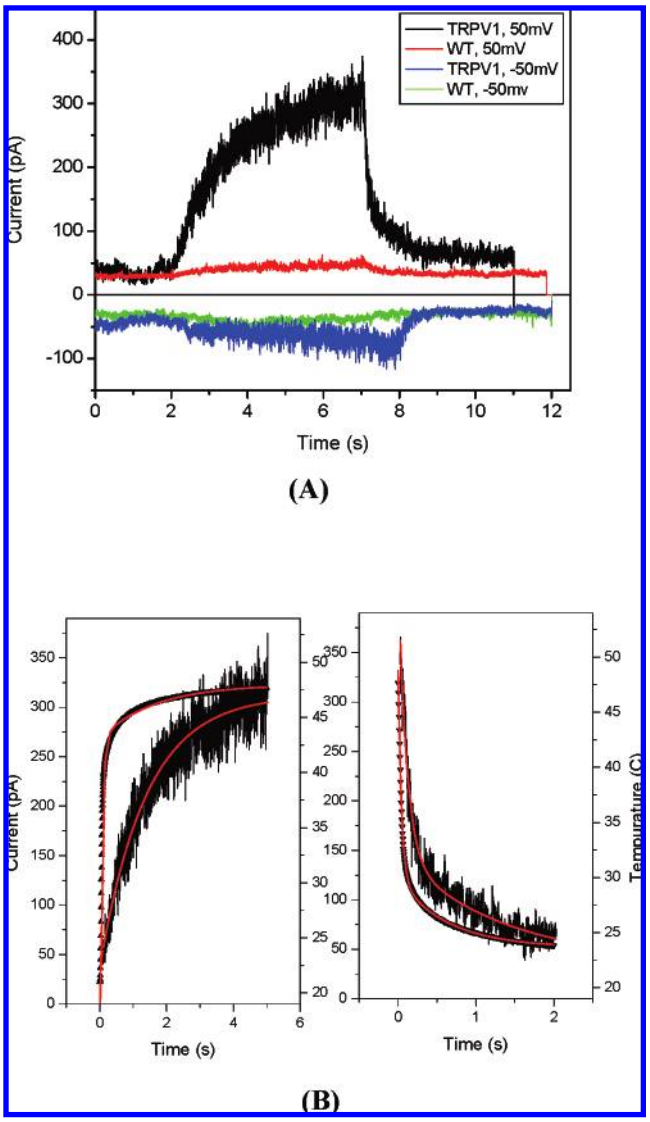

Figure 5. (A) Whole-cell patch-clamp recording of membrane current in response to a temperature pulse from room temperature to 45 °C: black, transfected cells at 50 mV; red, nontransfected cells at 50 mV; blue, transfected cells at −50 mV; green, nontransfected cells −50 mV. A flow rate of ∼11 mL/min was used for the entire experiment. (B) Curve fitting to recorded whole-cell current changes (left axis) in response to a temperature pulse (right axis). Left and right panels show temperature rise and drop, respectively.

conductance[20] as a function of temperature or using fluctuation analysis to estimate the unit conductance.[21]

Chip Characterization. The chip properties were characterized as a function of power at various flow rates. A series of voltage pulses 20 s wide with various amplitudes were applied to the heater while the temperature change was recorded using the Pt resistor. Figure 4A shows the temperature profile at the channel outlet for heater power ranging from 7.2 to 256 mW at a flow rate of 16.2 μL/min. This range of input power produced temperatures ranging from 20 to 70 °C at the channel outlet. Higher heater power produced both a greater temperature rise and a faster rate of rise (larger dT/dt) (see the Supporting Information). In addition, feedback may be used to improve the rise time.

Flow rate is the primary parameter that governs the temperature rise of the water. The temperature response for flow rates ranging from 6.1 to 34 μL/min is shown in Figure 4B when the heating power is at 113 mW. Lower flow rates resulted in larger increases in fluid temperature (Figure 4B) due to the longer times that fluid elements remain in contact with the heater. Figure 4C

(19) Auerbach, A.; Sachs, F.; Neil, J.; McGarrigle, R. *Methods in Enzymology, 124 Neuroendocrine Peptides*; Conn, P. M., Ed.; Academic Press: New York, 1986; p 190.
(20) Hodgkin, A. L.; Huxley, A. F. *J. Physiol. (London)* **1952**, *117*, 500.
(21) Colquhoun, D.; Hawkes, A. G. *Proc. R. Soc. London, Ser. B* **1977**, *199*, 231.

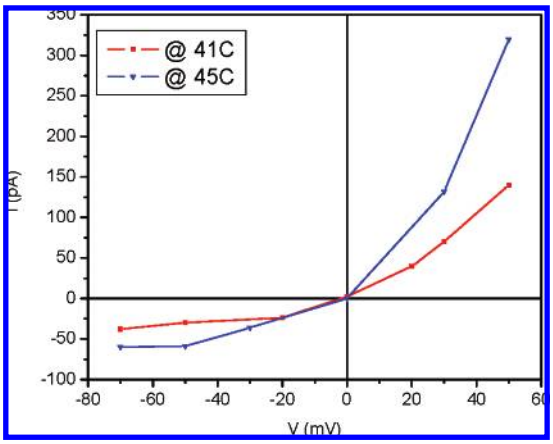

Figure 6. Current−voltage curve of the amplitude of the whole-cell current.

is an expanded view of the sensor response to the leading edge of hot fluid it receives from the heater. The results indicate that at slower flow rates it takes longer for the fluid to go from the heater to the sensor and, hence, a longer delay time. The dashed line in Figure 4C shows the temperature change sensed when there is no fluid flow. Since heat flows only by diffusion, this response defines the lower limit on heating rate. The difference between this curve and those with flow gives a good estimation of the contribution of fluid flow to the thermal response.

The variations of peak fluid temperature and rate of temperature rise as functions of the heater power and fluid flow rate are summarized and shown in Supporting Information, Figure S1. Both the peak temperature and the rate of rise are seen to vary linearly with heater power. As shown in Figure S1, the maximum rate of temperature rise was 0.8 °C/ms and occurred for the highest power input. When experiments are run in an open-loop control mode, the rate of temperature rise needs to be optimized via adjustments in both the heater power and fluid flow rate. On the other hand, operating in a closed-loop control mode will minimize both the set-point errors and the rise time. The patch-clamp experiments were conducted at 11 μL/min and with a rate of temperature rise of ∼0.5 °C/ms.

Patch-Clamp Studies. To demonstrate the performance of the thermal chip for patch-clamp experiments we examined TRPV1 transfected HEK293 cells. Figure 5A shows the whole-cell currents in response to heat stimulation for TRPV1 transfected and nontransfected cells. At 50 mV, increasing the temperature from 22 to 45 °C increased the current by ∼280 pA in the transfected cell, but only ∼20 pA in the control cell. Changing the holding potential to −50 mV produced an increase of the current of −53 pA in the transfected cell and less than −10 pA in the nontransfected cell, consistent with the expected heat activation of TRPV1 (Figure 5A). The time constant of the thermally activated current and the temperature rise were obtained by least-squares fitting to the data (Figure 5B). The time constant of current increase was ∼3000 ms, while the temperature rise time was ∼64 ms, so the chip is well capable of studying activation kinetics. The channel closure rate was comparable to the rate of change of the temperature and thus could not be studied in detail. Recently, Voets et al. used voltage jumps to relax the channel and estimated for a two-state model, the closing rate was in the range of 446−890 s^{-1} between 25 and 42 °C (see the Supporting Information in ref 22). This suggests that we would see the same rates with temperature jumps. However, if temperature acts on different domains than voltage, such as the lipids, the two measures may differ.

The whole-cell current was recorded over a range of potentials from −70 to 70 mV at different temperatures. Figure 6 shows steady-state current−voltage curves in response to two stimuli, 22−41 °C and 22−45 °C. These results are consistent with previously published data about TRPV1 channels.[23−25]

CONCLUSIONS

We have developed a microfluidic on-chip temperature stimulator for temperature-sensitive ion channel studies. The device is capable of rapidly switching solution temperature with a jump rate of >0.5 °C/ms. The effect of fluid flow on the temperature change was studied systematically with lower flow rates resulting in a higher temperatures and higher rise times. The patch-clamp studies showed that increasing temperature increased the conductance of the patch and of the open channel and the time constant of the patch's response to temperature is much slower than the chip rise time permitting kinetic studies. With the use of the same approach, the thermal chip can be used to build temperature controllable reactors for various biochemical assays and chemical reactions.

ACKNOWLEDGMENT

This work was supported by an NIH/STTR Grant through ALA Scientific Instrument, Inc. and partially supported by the National Science Foundation Grant No. CMS-0509723 and the NIH (F.S.). This work was performed, in part, at the Cornell Nanofabrication Facility, which is supported by the National Science Foundation Grant No. ECS-9731293.

SUPPORTING INFORMATION AVAILABLE

Additional information as noted in text. This material is available free of charge via the Internet at http://pubs.acs.org.

Received for review October 20, 2007. Accepted January 12, 2008.

AC702169T

(22) Voets, T.; Droogmans, G.; Wissenbach, U.; Janssens, A.; Flockerzi, V.; Nilius, B. *Nature* **2004**, *430*, 748−754.
(23) Caterina, M. J.; Schumacher, M. A.; Tominaga, M.; Rosen, T. A.; Levine, J. D.; Julius, D. *Nature* **1997**, *389*, 816−824.
(24) Benham, C. D.; Gunthorpe, M. J.; Davis, J. B. *Cell. Calcium* **2003**, *33*, 479−487.
(25) Tominaga, M.; Caterina, M. J.; Malmberg, A. B.; Rosen, T. A.; Gilbert, H.; Skinner, K.; Raumann, B. E.; Basbaum, A. I.; Julius, D. *Neuron* **1998**, *21*, 531−543.